Integrated flow sensor for in situ measurement and control of acoustic streaming in flexural plate wave micropumps

Nam-Trung Nguyen [a,*], Audra H. Meng [b], Justin Black [b], Richard M. White [b]

[a] *School of Mechanical and Production Engineering, Nanyang Technological University, Nanyang Avenue, Singapore 639798, Singapore*
[b] *Berkeley Sensor and Actuator Center, Department of Electrical Engineering and Computer Sciences, University of California at Berkeley, 497 Cory Hall, Berkeley, CA 94720, USA*

Abstract

This paper presents the design, fabrication, and characterization of a micromachined flow sensor, which is integrated onto the flexural plate wave (FPW) micropump. The flow sensor and the FPW micropump represent a complex microfluidic system that is able to control the fluid flow in the device. The system was designed using a commercial software package. The microfluidic system of a size of 10×10 mm was fabricated using common fabrication techniques. The micropump is made of an aluminum, piezoelectric zinc oxide, polysilicon, and low-stress silicon nitride membrane with a typical thickness of $1-3$ µm. The thermal flow sensor consists of a polysilicon heater and polysilicon–aluminum thermopiles as temperature sensors. The cold junctions of the thermopiles are located in a new design that will avoid the drift effect of the flow sensor. The results show expected flow velocity–drive voltage characteristics. © 2000 Elsevier Science S.A. All rights reserved.

Keywords: Microfluidic system; Thermal flow sensor; Micro pump; Acoustic streaming

1. Introduction

Recently, microfluidic systems have emerged as an important research topic. Applications in microbiology and micro chemical analysis motivate the development of microfluidic systems that can control and deliver different fluids in nanoliter to microliter ranges. Numerous papers have been published focusing on the development of micro pumps and micro flow sensors. Some overviews of classical fluidic components can be found in Refs. [1–3]. Because of the backpressure dependency of the flow, there is a need to control the pumping performance in order to maintain a constant flow rate. Gass et al. reported a hybrid system that can regulate flow rate up to 100 µl/min against backpressure up to 100 mbar [4]. Very few works presented a complex integrated system. Lammerink et al. [5] presented a system with an integrated thermal actuated micropump and a thermal flow sensor for flow rates on the order of 10 µl/min. Pumps with flow rates on the order of 1 µl/min were not reported.

In recent years, considerable attention has been focused on the use of flexural plate wave (FPW) devices for pumping fluids. This pumping principle enables the realization of an ''active'' micro channel and overcomes the high impedance encountered during delivery of fluid through channels.

Several papers have proven the possibility of using the FPW device as a micro-pump for submicroliter per minute flow rates [6–8]. The device presented in this paper consists of a flow sensor and an FPW micropump. The device is a first complex microfludic system with an FPW pump.

Fig. 1 shows the structure of the microfluidic system described in this paper. The device consists of a rectangular flow channel that has a thin membrane on the bottom. The membrane is made of piezoelectric zinc oxide, aluminum, and low-stress silicon nitride, and has a typical thickness d_M of $1-3$ µm. With an FPW length λ of 100 µm, the drive frequency f is in the range of $3-5$ MHz. Arrays of finger pairs placed at wavelength intervals termed interdigital transducers (IDTs) generate the plate waves. The flow sensor is integrated on the same membrane. The sensor consists of a polysilicon heater and temperature

---

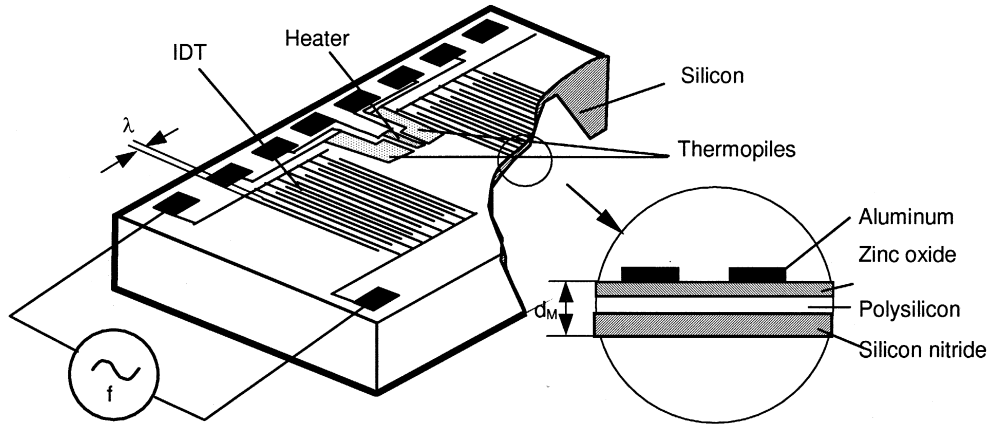* Corresponding author. E-mail: namtrungnguyen@yahoo.com

Fig. 1. The device with an FPW pump and a flow sensor.

sensors for detecting shifts of the temperature profile on the membrane.

2. Design of the device

2.1. Design of the FPW pump

The simulation utilizes the moving grid facilities of a commercial CFD software package (CFDRC Cooperation). A user library routine written in FORTRAN modifies the grid positions [9]. Essential parameters of the model such as the current time and grid positions can be specified from predefined constants and routines. The pressure field and the first-order velocity field of each time step are saved and used as the initial condition for the next time step. The vertical displacement Δz (perpendicular to the membrane), the horizontal displacement Δx (wave propagation direction), are given by:

$$\Delta z = A\sin(\omega t - kx), \tag{1}$$

$$\Delta x = \frac{A\pi d_M}{\lambda}\cos(\omega t - kx), \tag{2}$$

where A is the wave amplitude, $\omega = 2\pi f$ is the angular frequency of the wave, $k = 2\pi/\lambda$ is the wave number, and d_M is the membrane thickness. The time-averaged velocity field can then be calculated and depicted using MATLAB (Fig. 2). Details of the simulation results were described in Ref. [10].

In order to optimize the design of the FPW device for the best pumping performance, two parameters were investigated: the wave amplitude and the channel height.

Fig. 3 depicts the velocity profile and the peak velocity vs. the wave amplitude in a 50-μm channel. The curve at the bottom represents the parabolic characteristic of the maximum velocity. Enlarging the wave amplitude increases the time-averaged velocity over the entire channel. The results here give an unequivocal behavior of the pumping performance that the flow rate varies as the

square of drive voltage, which is proportional to the wave amplitude. Therefore, the wave amplitude, and consequently the drive voltage, are the most important parameters for controlling the flow rate of the pump.

Results of the velocity profile in channel with different heights and an wave amplitude of 10 nm are shown in Fig. 4. The bottom curve is the peak velocity of each profile. It shows clearly that the maximum velocity stays constant with a channel height greater than the evanescent decay distance (~ 20 μm). Therefore, channels with heights greater than twice the evanescent decay distance of the acoustic field have equal volume flow rates.

The results also show that velocity increases substantially in channels with height less than the decay length of the acoustic evanescent. In such channels, the velocity has a parabolic profile with high peak velocities.

2.2. Design of the thermal flow sensor

The design of the thermal flow sensor is based on the analytical model described in [11]. With the temperature
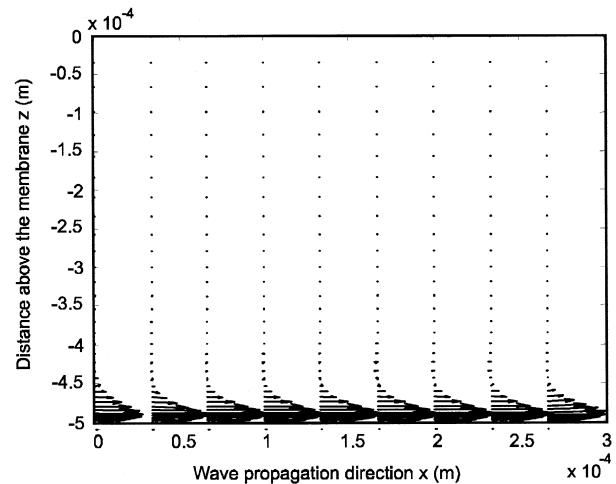

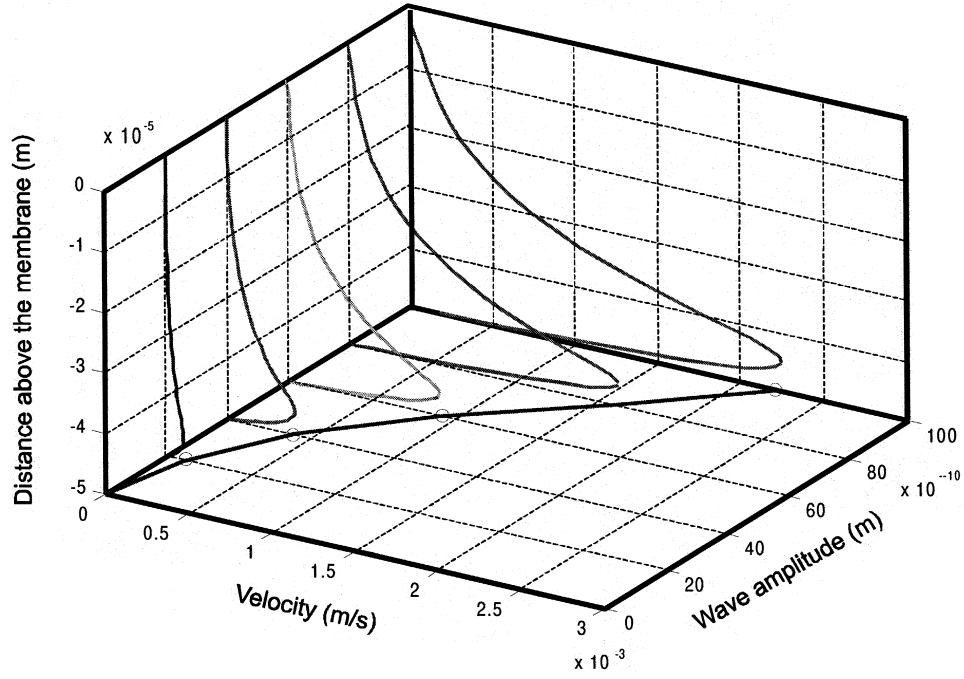Fig. 2. Velocity field of the acoustic streaming in air (plate wave amplitude, 6 nm).

Fig. 3. Velocity profile of water over the channel height of 50 μm driven by different wave amplitudes.

along the flow direction ϑ, the average flow velocity v, the thermal conductivities of the membrane λ_M and of fluid λ_{Fl}, the thermal diffusivity of fluid a_{Fl}, the constant thickness of the thermal boundary layer δ, the thickness of the membrane d_M and the distances of the temperature sensors to the heater upstream l_u and downstream l_l, we get the temperature difference $\Delta\vartheta(v)$ between the temperature sensors:

$$\Delta\vartheta(v) = \vartheta_0\left[\exp(\gamma_2 l_u) - \exp(-\gamma_1 l_l)\right] \tag{3}$$

with:

$$\gamma_{1,2} = \frac{v \pm \sqrt{v^2 + 16a_{Fl}^2\kappa/\delta^2}}{4a_{Fl}\kappa} \tag{4}$$

The dimensionless factor:

$$\kappa = \frac{1}{2} + \frac{\lambda_M d_M}{\lambda_{Fl}\delta} \tag{5}$$
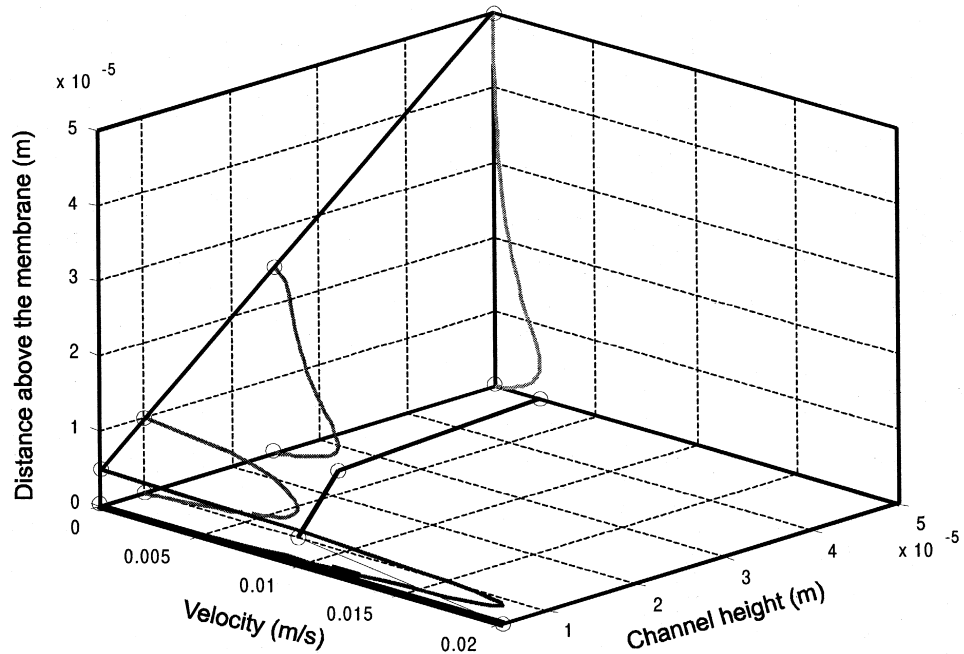

Fig. 4. Velocity profile of water with different channel heights driven by a wave amplitude of 10 nm.

describes the influence of the diaphragm material on the heat balance. The heater temperature at a constant heat power P is calculated with:

$$\vartheta_0 = \frac{P}{\lambda_{Fl} b_H \left[l_H/\delta + \sqrt{(v^2\delta^2)/(4a_{Fl}^2) + 4\kappa} \right]} \qquad (6)$$

Results of this model and former investigations [12] show that the sensor signal is proportional to a small flow rate, which is the case of the acoustic streaming in the FPW pump.
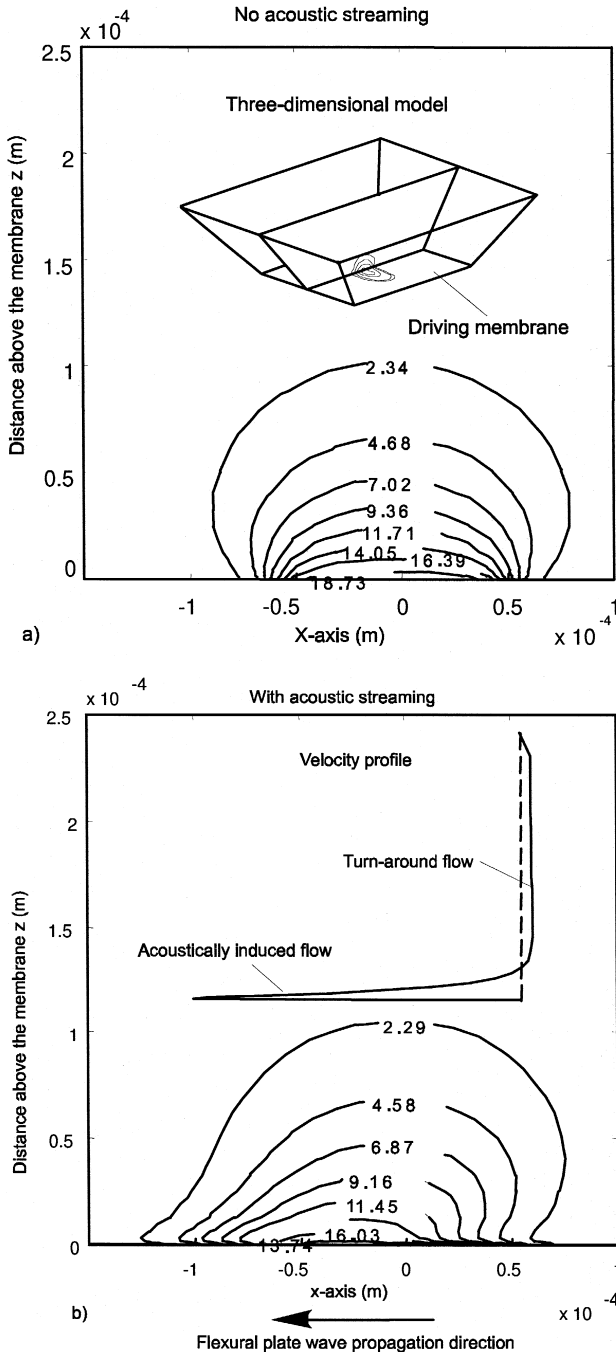

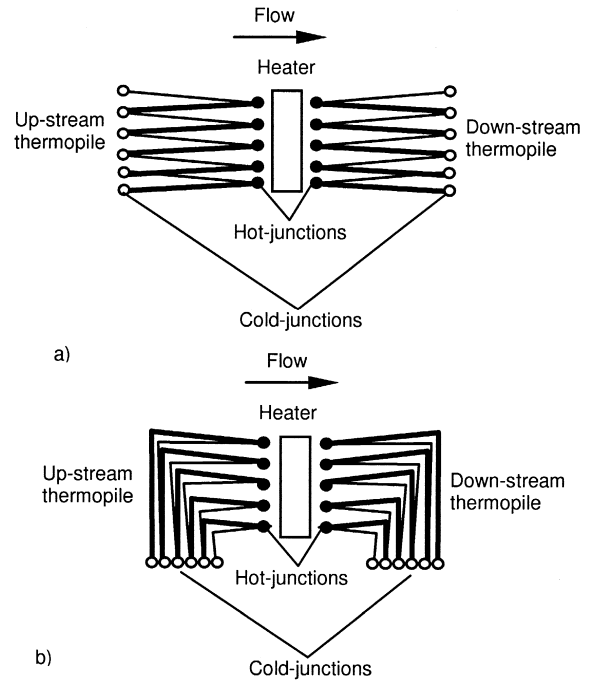Fig. 5. Temperature profile in fluid without acoustic streaming (a) and with acoustic streaming (b).

Fig. 6. Principle of the thermopile–heater–thermopile arrangement in a thermal flow sensor: (a) classical design, (b) new design for improvement of long-time stability.

Using the same simulation tool described above, the influence of the acoustic streaming on the temperature profile in the fluid can also be predicted. Fig. 5 shows the simulation results in a closed device using a three-dimensional model. The model shown in Fig. 5a has a actuating membrane at the bottom. All other sides of the model are set as walls. Since the device is closed, there is a turn-around flow at the top of the channel (Fig. 5b). Without the acoustic streaming, the temperature profile shown in Fig. 5a is symmetrical. With the acoustic streaming, the temperature profile indicates clearly the acoustic induced flow close to the actuating membrane, and the turn-around flow at the top of the channel (Fig. 5b).

The design of the flow sensor considers drift-effects of the thermal flow sensors based on thermopiles. In all published works, the cold junctions of thermopiles are located in the flow direction (Fig. 6a). That means the fluid transports the thermal energy directly from the heater to the cold junctions of the down-stream thermopiles. After a while in operation, the fluid will elevate the temperature of the cold junctions. This effect causes the drift of the sensor signal. In our design, the cold-junctions are located sideward, out of the influence of the thermal transfer (Fig. 6b). This new arrangement promises a better long-time behavior of the flow sensor.

3. Fabrication

The fabrication sequences for the microfluidic system are sketched in Fig. 7. Starting with a $\langle 100 \rangle$ silicon wafer, the membrane was fabricated by coating a thick LPCVD
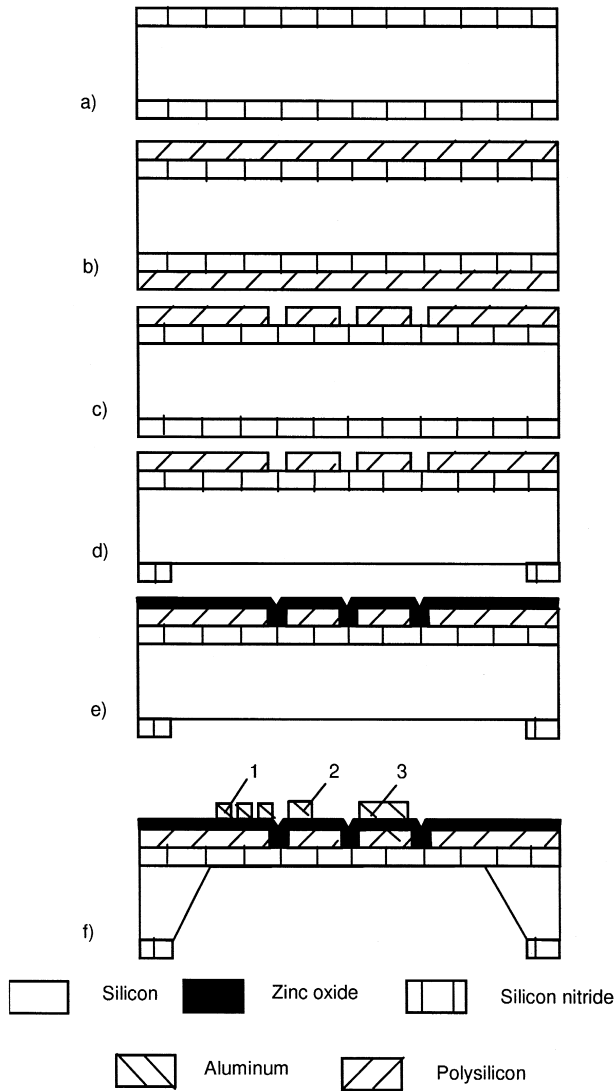
Fig. 9. Acoustic streaming velocities in water vs. wave amplitude. +: experimental results of 15-μm channel, ×: experimental results of 500-μm channel.

then patterned and etched in order to form the heater and the first part of the temperature sensors (Fig. 7c). Afterwards, the silicon nitride layer of the backside was opened with dry etching, in preparation for membrane formation (Fig. 7d). After the RF magnetron-sputtering of the zinc oxide layer, the contacts to the polysilicon were opened by patterning and etching the zinc oxide (Fig. 7e). Thereafter, aluminum was sputtered and structured in order to fabricate contacts to the heater, aluminum parts of the thermopiles and the interdigitated electrodes. Finally, the FPW membrane was freed by etching the silicon with KOH (Fig. 7f). The fabricated device is shown in Fig. 8.

4. Experimental results

For validating the pumping performances, the device was tested with water. Flow velocity measurement was

Fig. 7. Fabrication sequences of the micro fluidic system: (1) interdigitated electrode, (2) thermopile, (3) heater.

low-stress silicon nitride layer (Fig. 7a), and a polysilicon layer subsequently (Fig. 7b). The polysilicon layer was
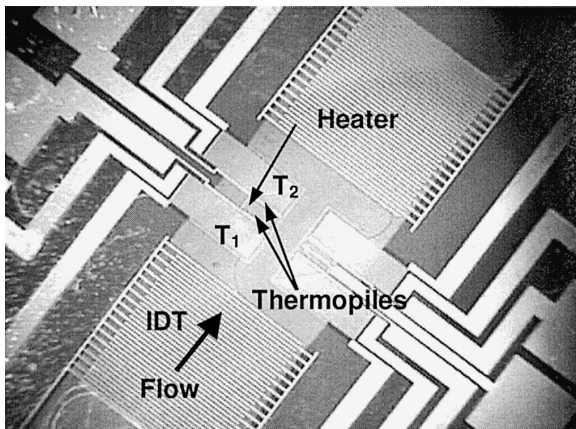

Fig. 8. The fabricated microfluidic system with integrated FPW pump and thermal low sensors.
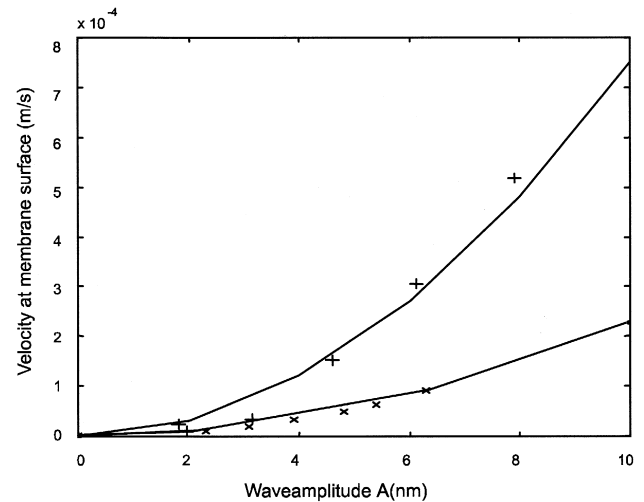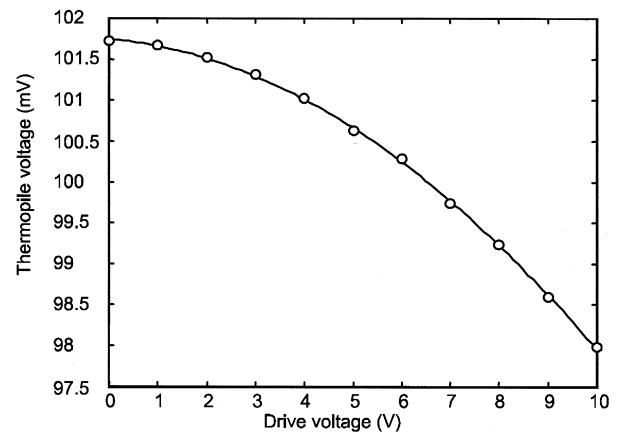

Fig. 10. Thermopile voltages (heater temperature) vs. drive voltages (wave amplitudes) in hot-film mode with 8.4 mW heat power (measurement in air).
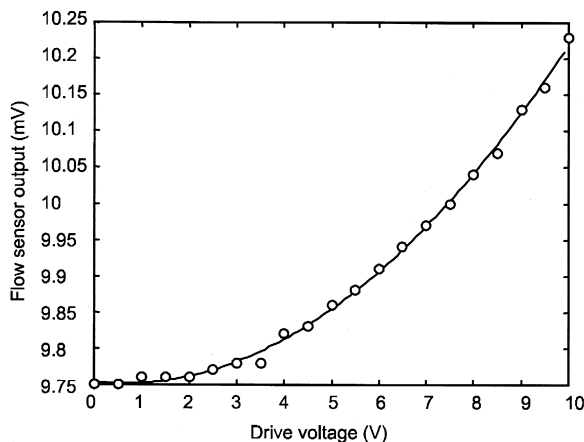
Fig. 11. Flow sensor signals (flow velocities) vs. drive voltages (wave amplitudes) in electrocaloric mode with 3.1 mW heat power (measurement in air).

carried out using 2-μm polystyrene spheres in devices with 500- and 15-μm channel height. Results in Fig. 9 show the velocities of the spheres has the quadratic behavior as expected in the numerical simulation (see Fig. 3). The solid lines in Fig. 9 indicate the simulation results that are corrected by factor 7 in order to fit the slower particle velocities. The wave amplitude was measured using the laser diffraction method [6]. Second, the thermopile performance was characterized. The results showed a linear behavior of the thermopile output.

The performance of the flow sensor and the FPW pump was then tested in air. The device was protected with a cover in order to minimize airflow from the surrounding environment. The heat power was kept under 10 mW because of the disturbance of the turbulent free convection at high temperature.

The thermal flow sensor was operated in two modes: the hot-film mode and the electrocaloric mode [12]. In the hot-film mode, the cooling of the heater at a constant heating power was measured. The heater temperature gives information about the flow. In the electrocaloric mode, the difference in fluid temperature up- and downstream of the heater $T_2 - T_1$ (Fig. 8) indicates the bypassing flow. Fig. 10 illustrates the temperature of the heater's left side vs. the drive voltages of the IDTs at a constant heating power. The cooling characteristics have a typical quadratic behavior.

In the electrocaloric mode, the voltage difference between thermopiles up- and downstream of the heater is used as the sensor signal. For low flow rates, the sensor signals is proportional to the flow velocity [12]. The sensor output–drive voltage characteristics are shown in Fig. 11. The flow velocity–wave amplitude characteristics have a quadratic behavior. In both Figs. 10 and 11, circles are measurement points, lines are fitting curves.

5. Conclusions

We have presented and proven the performance of a thermal flow sensor integrated in an FPW device for in situ measurement and control of acoustic streaming. The acoustically driven micropump offers the advantages of low operating voltages and gentle pumping with no valves involved. The pump is especially suitable for delivering cells and other sensitive biomaterials. The thermal flow sensor described in this paper is able to detect the relatively slow velocity of the acoustic streaming. Further calibration works should be carried out in order to use the sensor for detecting the small volume flow rate. The experimental results show the possibility of a closed-loop-controlled system, which has many applications. Potential applications include reagent transport in a micro total analysis system (μTAS), cell manipulating systems, and drug delivery systems.

Acknowledgements

References

[1] S. Shoji, M. Esashi, Microflow devices and systems, J. Micromech. Microeng. 4 (1994) 157–171.

[2] P. Gravesen, J. Branebjerg, O.S. Jensen, Microfluidics — a review, J. Micromech. Microeng. 3 (1993) 168–182.

[3] M. Elwenspoek, T.S. Lammerink, R. Miyake, J.H.J. Fluitman, Towards integrated microliquid handling systems, J. Micromech. Microeng. 4 (1994) 227–245.

[4] V. Gass et al, Integrated flow-regulated silicon micropump, Sens. Actuators A 43 (1994) 335–338.

[5] T.S. Lammerink et al., Integrated micro-liquid dosing system, Proc. MEMS '93, pp. 254–259.

[6] R.M. Moroney et al, Microtransport induced by ultrasonic Lamb waves, Appl. Phys. Let. 59 (1991) 774–776.

[7] P. Luginbuh, S.D. Collins, G.A. Racine, M.A. Gre'tillat, N.F. de Rooij, K.G. Brooks, N. Setter, Microfabricated Lamb wave device based on PZT sol–gel thin film for mechanical transport of solid particles and liquids, J. MEMS 6 (1997) 337–346.

[8] C.E. Bradley, R.M. White, Acoustically driven flow in flexural plate wave devices: theory and experiments, Proc. IEEE Ultrasonics Symp. (1994) 593–597.

[9] N.T. Nguyen et al., Computational Fluid dynamics modeling of flexural plate wave pumps, Proc. IEEE Int. Ultrasonics Symp. (1998), in print.

[10] N.T. Nguyen, R.M. White, Design and optimization of an ultrasonic flexural plate wave micro pump using numerical simulation, Sens. Actuators A 77 (1999) 231–238.

[11] N.T. Nguyen, W. Dötzel, Asymmetrical locations of heaters and sensors relative to each other using heater arrays: a novel method for designing multi-range electrocaloric mass flow sensors, Sens. Actuators A 64 (1997) 506–512.

[12] N.T. Nguyen, Micromachined flow sensors — a review, Flow Meas. Instrum. 8 (1997) 7–16.

Nam-Trung Nguyen was born in Hanoi, Vietnam, in 1970. He received his Dipl.-Ing. and Dr.-Ing. degrees in Electronic Engineering from Chemnitz University of Technology, Germany, in 1993 and 1997, respectively. During this time his research was focused on microfluidics. From 1996 to 1997, he has led the microfluidics group of the Department of Microsystems and Precision Engineering and the Center of Micro Technology focusing on microfluidic components and systems. In 1998, he worked as a postdoctoral research engineer in the Berkeley Sensor and Actuator Center (EECS, University of California Berkeley), where he was involved with research on microfluidic systems based on FPW devices. Since June 1999, he is affiliated with the School of Mechanical and Production Engineering of the Nanyang Technological University in Singapore. Dr. Nguyen has published several journal articles on microfludics. He is also the co-author of two books in German and in English. His book on the fundamentals of microsystem technology was published recently in Vietnamese.

Audra Meng is a doctoral student in the joint bioengineering program at the University of California at Berkeley and the University of California at San Francisco, and plans to finish her degree by December 1999. She received her B.S. degree from the California Institute of Technology in electrical engineering. Her research interests include the use of micro-electrical–mechanical systems (MEMS) for applications in biology and medicine.

Justin Black was born in Seattle, WA in 1973. He is presently pursuing his PhD with the Berkeley Sensor and Actuator Center, researching applications of ultrasonics in microfluidic systems.

Richard M. White is a professor in the electrical engineering and computer sciences department at the University of California, Berkeley. After obtaining his bachelor's, masteral and doctoral degrees in engineering science and applied physics at Harvard, he worked on microwave devices at the General Electric Microwave Laboratory in Palo Alto. He moved to Berkeley where he has taught and carried out research on solid-state sensors. He is a director of the Berkeley Sensor and Actuator Center, an IEEE Fellow, and a member of the National Academy of Engineering.